Local density of states of chiral Hall edge states in gyrotropic photonic clusters

Ara A. Asatryan,[1,*] Lindsay C. Botten,[2] Kejie Fang,[3] Shanhui Fan,[3] and Ross C. McPhedran[4]

[1]*Department of Mathematical Sciences, University of Technology, Sydney NSW 2007, Australia*
[2]*Department of Mathematical Sciences and the Centre for Ultrahigh-bandwidth Devices for Optical Systems (CUDOS),*
University of Technology, Sydney NSW 2007, Australia
[3]*Department of Electrical Engineering, Stanford University, Stanford, California 94305, USA*
[4]*School of Physics and CUDOS, University of Sydney, Sydney NSW 2006, Australia*

We have constructed the Green's tensor for two-dimensional gyrotropic photonic clusters and have calculated their optical local density of states (LDOS). For clusters that support the chiral Hall edge states we calculate the LDOS as a function of wavelength, position, size, and shape of the cluster. It is shown that the LDOS of Hall edge states is a strong function of the cluster shape and position. The LDOS can be orders of magnitude higher at the edges of the cluster compared to the free space value while it vanishes towards the cluster center. It is shown that the LDOS in such photonic clusters can withstand a very strong disorder due to their topological protection. The spatial profiles of chiral Hall edge modes, their quality factors, and their excitations have been calculated. Both gyroelectric and gyromagnetic (ferrite) clusters have been treated.

PACS number(s): 42.70.Qs, 42.25.Gy

I. INTRODUCTION

Analogies between solid-state physics and optics have turned out to be very productive. One of the examples of this is the field of photonic crystals.[1] Such materials are sometimes called semiconductors for photons owing to the strong resemblance between optical and electronic band structures. The properties of such artificial periodic nanomaterials can be exploited to miniaturize optical components leading to compact energy-efficient optical devices.

One of the well-known fundamental effects in solid-state physics is the integer quantum Hall effect (QHE).[2–5] It has been discovered that the Hall conductance of two-dimensional metallic samples at low temperatures in a magnetic field is quantized in multiples of the ratio e^2/h. This led to the establishment of an electrical resistance standard and unprecedentedly accurate measurement of the fine-structure constant $\alpha = e^2/hc$. One of the fundamental features of the QHE is the existence of chiral edge states. This property has been recognized early[5] and has been used to characterize the Hall conductance in Landauer's formalism. At first sight it is hard to assume that chiral Hall edge states can exist for photons, where there are no Landau levels in the presence of a magnetic field, and photons are bosons in contrast to fermionic electrons. However, these differences have been proven to be not essential.[6] What is crucial instead is the breaking of time-reversal symmetry which leads to the realization of the QHE in electronic systems without the necessity of a static magnetic field. This finding paves the way for the possibility to have an analog of the chiral Hall edge states for photons.

Recently the existence of the photonic chiral states have been pointed out in beautiful papers by Haldane and Raghu[7,8] where they proposed to use photonic crystals made of optically active materials possessing Dirac points in their dispersion diagrams at the absence of the magnetic field. Subsequently it has been shown theoretically that one-way edge states can exist in photonic crystals with gyrotropic components, even without Dirac points[9] and experimentally observed by Wang *et al.*[10] In these geometries[7–10] the one-way edge states exist at the interface of two photonic crystals where the Chern number—

the topological invariant of a band[11]—changes across the interface. The second photonic crystal here acts like a mirror and thus provides the confinement of the one-way edge state given that the edge states lie inside the light cone. It turns out that the one-way edge state can exist also at the interface of a gyrotropic photonic crystal and free space provided that the one-way edge states lie below the light cone.[12]

Similar one-way electromagnetic modes exist as a one-way surface plasmon when a metal is subject to a strong magnetic field,[13] at the edges of a photonic crystal ribbon with infinite extent in transverse directions,[14] or even in coupled plasmonic particle chains,[15–17] and at the interface of two gyrotropic media with opposite magnetization.[18] Such strong interest in the properties of photonic chiral Hall edge states is based on their intrinsic properties, immunity to backscattering and disorder. This makes them an ideal candidate for the development of robust nanoscale waveguides and interconnects. Therefore, it is important to understand their fundamental properties. A microscopic theory of chiral Hall edge states has been developed in the tight-binding approximation,[19] where the connection between the one-way edge modes and the bulk modes has been established.

So far the research has been concerned mainly with the establishment of the existence of the chiral Hall edge states in different photonic systems with an infinite or semi-infinite extent, with the exception of Ref. 12. However, all realistic photonic structures are finite and therefore it is necessary to investigate the properties of the chiral Hall edge modes in finite photonic clusters. Knowledge of the spatial profiles and quality factors of these chiral edge modes, their dependencies on the shape of the cluster, as well as their excitations are very important in potential applications. It is important also to investigate the radiation properties of sources embedded in such structures. These properties are determined by their local density of states, which is given by the imaginary part of the trace of the electromagnetic Green's tensor.[20,21]

The purpose of this paper is twofold. The first is to construct the Green's tensor in finite photonic gyrotropic clusters which support chiral Hall edge states, and to characterize their local

density of states (LDOS). The second is to calculate the spatial profiles of chiral Hall edge states, their quality factors, and their excitations. We also present the effects of disorder on LDOS of one-way Hall edge states. We consider both gyroelectric and gyromagnetic (commonly known as ferrites) photonic clusters composed of circular cylinders of infinite extent.

In Sec. II we outline the construction of the Green's tensor of gyrotropic photonic clusters based on the multipole approach. In Sec. III we present the numerical results of the LDOS calculations of gyroelectric and ferrite photonic clusters. Then, we present the results of the spatial profile calculations of chiral Hall edge modes, their quality factors, and their excitations. Finally, we consider the effects of disorder on the LDOS.

II. ANALYTICAL TREATMENT

In this section we outline the application of the multipole method to construct the Green's tensor for two-dimensional ferrite and gyroelectric photonic clusters composed of cylinders with circular cross sections, and to calculate their LDOS. The method of calculation of chiral Hall edge mode profiles and their quality factors is also given. The details of the derivation will be presented elsewhere. To construct the Green's tensor we apply the multipole technique[22] proven to be highly efficient and accurate.[23,24] The LDOS can be calculated from the imaginary part of the Green's tensor,[20,21]

$$\rho(\mathbf{r}; \omega) = -4 \text{ImTr}\big[\mathbf{G}^e_{\alpha\beta}(\mathbf{r}, \mathbf{r}; \omega) \big], \qquad (1)$$

where $\mathbf{G}^e_{\alpha\beta}(\mathbf{r}, \mathbf{c}_s; \omega)$ is the 3×3 electric field Green's tensor for an observation point at $\mathbf{r}$ and a source point at $\mathbf{c}_s$. The columns of the Green's tensor $[G^e_{x\beta}, G^e_{y\beta}, G^e_{z\beta}]$ are generated by a source parallel to axes $\beta = x, y, z$. In Eq. (1) the LDOS is normalized to its free space value.

The geometry of the problem consists of N_c nonoverlapping monotype gyrotropic cylinders aligned along the z axis with radii a_l and located at the positions $\mathbf{c}_l$ and with the dispersive tensorial material parameters $\hat{\varepsilon}_l(\omega)$ and $\hat{\mu}_l(\omega)$. The cylinders are located in a gyrotropic background medium with material parameters $\hat{\varepsilon}_b(\omega)$ and $\hat{\mu}_b(\omega)$. The positions of the cylinders, their radii, and their material characteristics can be arbitrary. Although the material characteristics of cylinders and background media can be complex, in the numerical examples in Sec. III they are assumed to be Hermitian tensors. The time dependence we choose in the form $e^{-i\omega t}$, and we scale the magnetic field by the free space impedance Z_0, $Z_0 \mathbf{H} \to \mathbf{H}$.

The magnetic permeability tensor of a ferrite material is given by

$$\hat{\mu} = \begin{pmatrix} \mu_\perp & i\mu_{xy} & 0 \\ -i\mu_{xy} & \mu_\perp & 0 \\ 0 & 0 & \mu_\| \end{pmatrix} \qquad (2)$$

and the dielectric constant of a ferrite is a scalar ε. The dielectric permittivity tensor of a gyroelectric material has the form

$$\hat{\varepsilon} = \begin{pmatrix} \varepsilon_\perp & i\varepsilon_{xy} & 0 \\ -i\varepsilon_{xy} & \varepsilon_\perp & 0 \\ 0 & 0 & \varepsilon_\| \end{pmatrix} \qquad (3)$$

and the magnetic permittivity is a scalar μ. In (2) and (3) we have assumed the Voigt geometry where the external static magnetic field $\mathbf{H}_0$ is applied in the z-axis direction.

For this geometry, the polarizations are decoupled and the field is determined by a single component E_z for TM polarization and ferrite cylinders, while it is specified by the H_z component for the TE polarization and gyroelectric cylinders. The TE polarization for ferrite cylinders and the TM polarization for gyroelectric cylinders are not interesting and their solutions simply reduce to the known scalar case.[22] Therefore, for ferrite clusters we consider only the TM polarization, while for the gyroelectric cylinders we consider the TE polarization only.

Accordingly, for this two-dimensional geometry the Green's tensor for TM polarization reduces to a form involving only a single scalar $\mathbf{G}^e = E_z \delta_{uz}$, and the LDOS can be calculated from

$$\rho = -4 \text{Im}[E_z(\mathbf{r}, \mathbf{r}; \omega)], \qquad (4)$$

while for TE polarization the Green's tensor reduces to a 2×2 tensor

$$\mathbf{G}^e = \begin{pmatrix} G_{xx} & G_{xy} & 0 \\ G_{yx} & G_{yy} & 0 \\ 0 & 0 & 0 \end{pmatrix} \qquad (5)$$

and the LDOS we calculate from (1) where the Green's tensor is given by (5).

For the ferrite cluster, the electric-field component E_z is determined from the equation

$$\nabla^2 E_z(\mathbf{r}; \mathbf{c}_s) + k^2 n^2(\mathbf{r}) E_z(\mathbf{r}; \mathbf{c}_s) = -\delta(\mathbf{r} - \mathbf{c}_s), \qquad (6)$$

where $n^2(\mathbf{r}) = \varepsilon(\mu_\perp^2 - \mu_{xy}^2)/\mu_\perp$ takes the role of the refractive index. For the gyroelectric cluster the magnetic field H_z component of the Green's tensor is given by the solution of the equation

$$[\nabla^2 + k^2 n^2(\mathbf{r})] H_z(\mathbf{r}) = i\hat{\mathbf{z}} \cdot \{\nabla \times [\hat{\varepsilon}^{-1} \mathbf{u}\, \delta(\mathbf{r} - \mathbf{c}_s)]\}/k, \qquad (7)$$

where $n^2(\mathbf{r}) = \mu(\varepsilon_\perp^2 - \varepsilon_{xy}^2)/\varepsilon_\perp$ and $\hat{\varepsilon}^{-1}$ is the inverse of the dielectric tensor (3). To find all the components of the electric Green's tensor $\mathbf{G}^e$ (5) it is necessary to solve (7) for the two orientations of the source $\mathbf{u} = \mathbf{x}, \mathbf{y}$ and find the corresponding electric-field components from Maxwell's equation $\mathbf{E} = -\hat{\varepsilon}^{-1} \nabla \times \mathbf{H}/ik$. Equations (6) or (7) needs to be solved in order to construct the Green's tensor and to deduce the LDOS using (1) for the TE polarization or (4) for the TM polarization. The calculations of the spatial profiles of chiral Hall edge states are also found from the solutions of (6) or (7) but without the source terms.

To find a solution of the multiple scattering problem (6) or (7) we represent the exterior field in the background medium at cylinder l with local coordinates $\mathbf{r}_l = (r_l, \theta_l) = \mathbf{r} - \mathbf{c}_l$ in the multipole expansion

$$V(\mathbf{r}; \mathbf{c}_s) = \sum_{m=-\infty}^{\infty} \big[A_m^l J_m(kn_e r_l) + B_m^l H_m^{(1)}(kn_e r_l) \big] e^{im\theta_l}, \qquad (8)$$

while the interior field is

$$V(\mathbf{r}; \mathbf{c}_s) = \sum_{m=-\infty}^{\infty} \big[C_m^l J_m(kn_i^l r_l) + D_m^l H_m^{(1)}(kn_i^l r_l) \big] e^{im\theta_l}, \qquad (9)$$

where $V(\mathbf{r})$ represents either the E_z or H_z field and n_e and n_i^l are the refractive indices of the background medium and cylinder l, respectively. The coefficients $\mathbf{A}^l = [A_m^l]$ represent the local field at the vicinity of the lth cylinder originating from all other cylinders or external sources and $\mathbf{B}^l = [B_m^l]$ represent the outgoing field of the lth cylinder, while $\mathbf{C}^l = [C_m^l]$ represent the internal field of the cylinder l and $\mathbf{D}^l = [D_m^l]$ represent the field originating from an internal source of the lth cylinder. By applying Green's second theorem over the cluster, with a subsequent application of Graf's addition theorem, we derive a partitioned system of linear equations for the unknown multipole coefficients $\mathbf{B}^l$. With the introduction of the partitioned vector $\mathbf{B} = [\mathbf{B}^l]$ the linear system for the unknown coefficients $\mathbf{B}$ can be expressed as

$$(\mathbf{I} - \mathbf{RH})\mathbf{B} = \mathbf{Q}, \tag{10}$$

where $\mathbf{Q}$ represents the external or internal sources. This is an infinite system of equations and must be truncated in any numerical implementation. The number of retained multipole coefficients per cylinder determines the accuracy of the solution. The internal field expansion coefficients $\mathbf{C}^l$ are expressed in terms of $\mathbf{B}^l$ using boundary conditions which are satisfied exactly in this approach. The nonreciprocal behavior of the considered clusters originates from the boundary conditions. The boundary condition matrix for gyrotropic circular cylinders is diagonal as in the scalar case (see Ref. 22) but contains an additional term proportional to ε_{xy}. The explicit form of these relations will be given elsewhere. The external E_z field can be reconstructed from the global expansion

$$
\begin{aligned}
E_z(\mathbf{r}; \mathbf{c}_s) &= H_0^{(1)}(kn_e|\mathbf{r} - \mathbf{c}_s|)/(4i) \\
&+ \sum_{q=1}^{N_c} \sum_{m=-\infty}^{\infty} B_m^q H_m^{(1)}(kn_e|\mathbf{r}_q|)e^{im\arg(\mathbf{r}_q)}, \quad (11)
\end{aligned}
$$

where $\mathbf{r}_q = \mathbf{r} - \mathbf{c}_q$, while the internal field of the lth cylinder can be calculated using the local expansion (9). The reconstruction equation for the H_z field takes a similar form,

$$
\begin{aligned}
H_z(\mathbf{r}; \mathbf{c}_s) &= (Q_1 e^{i\arg(\mathbf{r} - \mathbf{c}_s)} + Q_2 e^{-i\arg(\mathbf{r} - \mathbf{c}_s)})H_1^{(1)}(kn_e|\mathbf{r} - \mathbf{c}_s|) \\
&+ \sum_{q=1}^{N_c} \sum_{m=-\infty}^{\infty} B_m^q H_m^{(1)}(kn_e|\mathbf{r}_q|)e^{im\arg(\mathbf{r}_q)}, \quad (12)
\end{aligned}
$$

and the internal H_z field of the lth cylinder can be calculated using the local expansion (9). The first term in (11) or (12) is absent when the source is located in one of the cylinders. Likewise the second term in (9) is absent if the source is in the background. All other field components are found from Maxwell's equations analytically.

The outlined multipole method is as efficient and accurate as for the scalar material case.[22] The singularity of Green's tensor is associated only with the source term and this is removed analytically in Eqs. (1) and (4) thereby leading to highly accurate results for the calculated LDOS values. The boundary conditions on each cylinder are satisfied exactly, facilitating convergence, and the calculation of the LDOS map requires only one matrix inversion. The generalized Lorentz reciprocity condition[25] $G_{\alpha\beta}^e(\mathbf{r}, \mathbf{c}_s, \mathbf{H}_0) = G_{\beta,\alpha}^e(\mathbf{c}_s, \mathbf{r}, -\mathbf{H}_0)$ holds with accuracy better than 10^{-10} in all our numerical examples in Sec. III.

To find the chiral Hall edge states it is necessary to find the null solutions of the generalized eigenvalue system,

$$(\mathbf{I} - \mathbf{RH})\mathbf{B} = \mathbf{0}. \tag{13}$$

This requires the vanishing of the determinant of the linear system, i.e.,

$$\det(\mathbf{S}^{-1}) = 0, \tag{14}$$

$$\mathbf{S}^{-1}(\lambda) = (\mathbf{I} - \mathbf{RH}). \tag{15}$$

This is equivalent to finding the poles of the scattering matrix $\mathbf{S}$ in the complex frequency ω plane, or equivalently in the complex wavelength plane $\lambda_p = \lambda_p' + i\lambda_p''$. All poles are located in the lower half of the complex frequency plane or equivalently in the upper half of the complex wavelength plane because of the causality condition.

The finite cluster is open, and therefore all modes are leaky. Their quality factors can be calculated using the ratio $Q = \lambda_p'/2\lambda_p''$, where λ_p' is the real part of the wavelength and λ_p'' is its imaginary part. The real part λ_p' defines the wavelength or the frequency of the mode while the imaginary part λ_p'' defines its quality factor Q. After the poles are found the application of the singular value decomposition to (13) determines the vector of the multipole coefficients $\mathbf{B}$ for all cylinders. The modal field can then be reconstructed using Eqs. (9), (11), or (12) without source terms, and all other field components are calculated analytically using Maxwell's equations. It is well known that the Green's tensor has a modal decomposition [see Eq. (II.12) in Ref. 20 or Eq. (3.5) in Ref. 21], but we will not consider this representation here.

III. NUMERICAL RESULTS

In this section we present the results of numerical calculations of the LDOS of chiral Hall edge modes as a function of wavelength, position, and cluster shape based on the method outlined in Sec. II. The spatial dependencies, quality factors, and excitations of chiral Hall edge modes are also presented. First we consider the gyroelectric photonic honeycomb cluster [see Fig. 1(a)], and then we present results for ferrite clusters in the shape of a finite honeycomb ribbon and a hexagonal-shaped honeycomb flake (see Fig. 9). The effects of disorder on the LDOS are also briefly discussed.

A. LDOS and chiral Hall edge modes in gyroelectric clusters

Here we study the properties of the LDOS and the chiral Hall edge modes in gyroelectric clusters. For this case we use the parameters and geometry reported in Ref. 19, in which it was shown that the one-way Hall states exist between the interface of two semi-infinite photonic crystal regions [see Fig. 1(a)]. The underlying photonic crystal structure has a hexagonal lattice of period d of air cylinders. The cylinders have a radius $a = 0.35d$ and are located in a uniform dielectric with $\varepsilon = 16$. The TE modes of this crystal have a complete band gap for wavelengths $3.390 < \lambda/d < 5.208$ [see the band diagram in Fig. 1(b)]. In the structure shown in Fig. 1(a) the top region consists of such a photonic crystal. The bottom crystal is the same as the top except that there are gyroelectric cylinders embedded in the hexagonal lattice, which themselves form a honeycomb lattice, with a lattice period $d' = 6d$ and
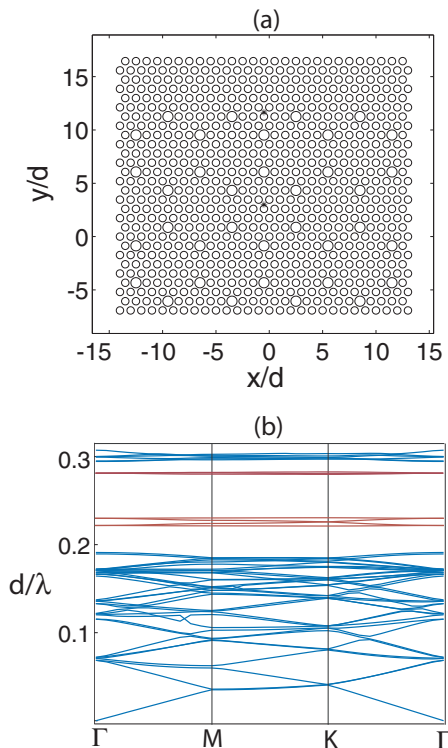
FIG. 1. (Color online) (a) The geometry of the gyroelectric cluster composed with $N_c = 770$ cylinders. In the corresponding semi-infinite photonic cluster the edge states are localized at the interface between the top five layers and the bottom gyroelectric cluster formed with $N_c = 633$ cylinders. (b) The band structure of a corresponding infinite photonic crystal embedded with honeycomb resonators.

radii $a = 0.5d$. These are cylinders with larger radii, as plotted in Fig. 1(a). The components of the dielectric tensor for gyroelectric resonators are $\varepsilon_\perp = 16$ and $\varepsilon_{xy} = 1$, while $\mu = 1$ throughout. Such a choice of parameters has allowed the application of the tight-binding approximation in Ref. 19. The typical value of ε_{xy} for available materials is of the order of 10^{-3} and presently there is an intense search to find ways in which this parameter can be enhanced. The dielectric tensor components $\varepsilon_\perp$ and ε_{xy} are functions of frequency and they have a form similar to the ferrites permittivity tensor components [see Eq. (16)]. It has been shown in Ref. 9 that the effect of the dispersion is not essential on the chiral Hall edge states and here we follow Ref. 19 and consider $\varepsilon_\perp$ and ε_{xy} as constants. The introduction of the honeycomb resonators with $\varepsilon_\perp = 16$ without magnetization $\varepsilon_{xy} = 0$ introduces new bands in the band gap [red bands in Fig. 1(b)] at $d/\lambda \approx 0.24$ and $d/\lambda \approx 0.29$.

The bands at $d/\lambda \approx 0.24$ are replotted in Fig. 2(a) with an enlarged scale as a function of the wavelength λ/d revealing the existence of a degenerate Dirac point at the K point of the Brillouin zone for the wavelength $\lambda/d \approx 4.44$. Using the λ/d scale will facilitate the subsequent comparison of the band diagram and the LDOS calculations. The introduction of gyrotropic resonators with $\varepsilon_{xy} = 1$ lifts the degeneracy and band gaps are opened up [see Fig. 2(b)] resulting in bands with nonzero Chern numbers.[7]
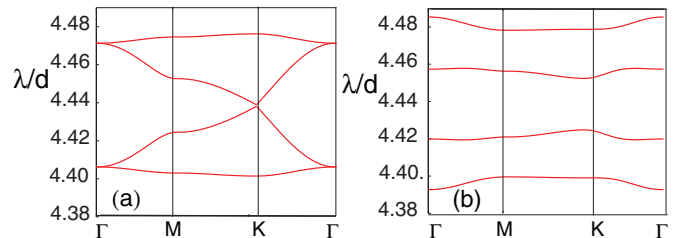

FIG. 2. (Color online) (a) A fragment of the band structure for a hexagonal photonic crystal with embedded microresonators without magnetization; (b) band structure for a hexagonal photonic crystal with embedded microresonators with magnetization.

In these situations the Hatsugai theorem[26] ensures the existence of chiral Hall edge states. Then the introduction of the top photonic crystal creates sufficient conditions for the existence of one-way Hall modes at the interface of the two regions. For more details, see Ref. 19.

Having reviewed the properties of semi-infinite structures, we now consider the properties of finite clusters. In Fig. 3 we plot the LDOS ρ on a logarithmic scale versus wavelength (the green dashed curve) for a finite hexagonal cluster of $N_c = 633$ air cylinders embedded in the background with $\varepsilon = 16$ and for a point located in the background near the center of the cluster with the coordinates $(-0.5, 2.89)$ [the bottom black dot in Fig. 1(a)]. This cluster is similar to the structure plotted in Fig. 1(a) but without the top five layers and without the embedded resonators in the bottom region. The LDOS for this cluster exhibits a clear photonic band gap in the wavelength range $3.40 < \lambda/d < 5.2$ consistent with the band-structure calculations. Within the gap the LDOS can be 10^9 times smaller than free space value.

The blue solid curve in Fig. 3 is the LDOS for the same point and the same hexagonal cluster but with embedded honeycomb resonators [see Fig. 1(a)]. The introduction of the honeycomb resonators in this finite cluster introduces two resonance regions at $\lambda/d \approx 3.5$ and $\lambda/d \approx 4.5$ inside the
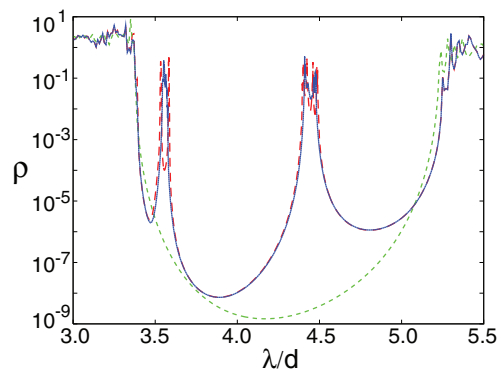

FIG. 3. (Color online) The LDOS ρ on a logarithmic scale versus wavelength λ/d for an observation point at $(-0.5; 2.98)$ located in the background for the cluster composed with $N_c = 633$ cylinders (bottom green dashed curve). The blue solid curve is the same as the green dashed curve but for a hexagonal cluster embedded with nonmagnetized honeycomb resonators and the red long dashed curve is the same as the blue curve but with gyroelectric resonators with radii $a = 0.48d$.
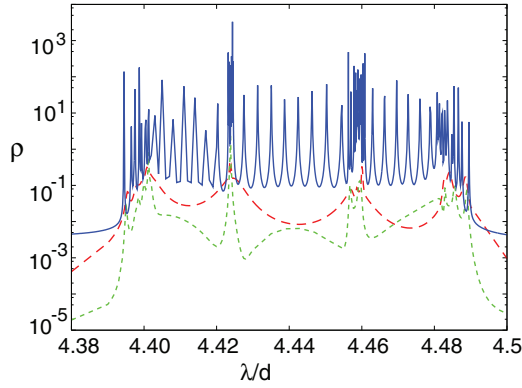
FIG. 4. (Color online) The red long dashed curve is the same red curve as in Fig. 3, while the green dashed curve is the LDOS for a gyroelectric cluster depicted in Fig. 1(a) and for a source point located at $(-0.5, 11.65)$ (top black dot). The blue oscillating curve is for the gyroelectric cluster with $N_c = 1007$ cylinders formed by placing four layer mirrors around the gyroelectric cluster composed with $N_c = 633$ cylinders and for the same observation point as the green dashed curve.
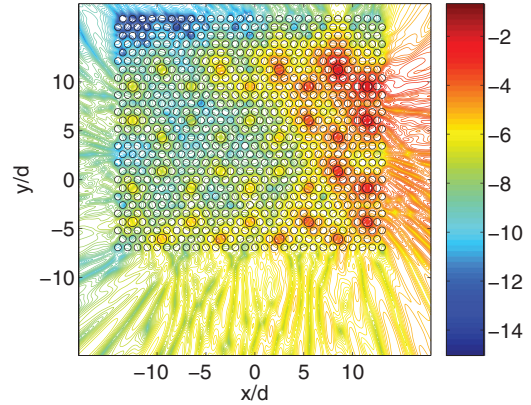

FIG. 5. (Color online) The intensity of the magnetic field distribution $|H_z|^2$ of the chiral Hall edge state in a logarithmic scale for the gyroelectric cluster depicted in Fig. 1(a) at $\lambda/d = 4.436 + i0.015$.

band gap which is consistent with the band structure shown in Fig. 1(a). The LDOS at the Dirac point $\lambda/d = 4.4$ [see Fig. 2(a)] of this finite cluster is two orders of magnitude lower than the free space value (see the blue curve at $\lambda/d \approx 4.4$ in Fig. 3), while for the infinite photonic crystal the LDOS at the Dirac point vanishes. We have calculated ρ for a larger cluster and have observed that ρ at the Dirac point is reduced accordingly.

The LDOS for the cluster with the embedded resonators has one peak at the first resonance region at $\lambda/d = 3.5$ and two peaks at the second resonance region at $\lambda/d = 4.5$ (see the blue solid curve in Fig. 3). The introduction of the magnetization splits these peaks in two. To see this more clearly we have replotted the vicinity of the second resonance region in Fig. 4. The red long-dashed curve in Fig. 4 is the same as the red curve in Fig. 3 and reveals these four resonance regions which correspond to the four bands of the infinite photonic crystal with embedded gyroelectric microresonators [see Fig. 2(b)]. The green dashed curve in Fig. 4 corresponds to the cluster with $N_c = 770$ cylinders depicted in Fig. 1(a) but for a point located at the interface of a cluster with gyroelectric microresonators and a "mirror" composed of five layers of a hexagonal photonic crystal for the point with the coordinates $(-0.5, 11.65)$ [top black dot in Fig. 1(a)].

The blue solid curve in Fig. 4 is the LDOS for a cluster composed with $N_c = 1007$ cylinders formed by placing mirrors composed of four layers of cylinders around the cluster with $N_c = 633$ cylinders and embedded gyroelectric resonators and for the same observation point as for the green dashed curve. The geometry of this cluster is plotted in Fig. 6. The introduction of the mirrors has a dramatic effect on the LDOS which now has a number of strong oscillations in this region. Surrounding a gyroelectric cluster with mirrors substantially confines the one-way modes. This shifts the poles of the scattering matrix toward the real axis therefore their quality factors are substantially higher and the one-way modes become "visible" in the LDOS plot as well developed oscillations. By

increasing the size of the cluster more poles move closer to the real axis leading to more oscillatory behavior of the LDOS. In the limit of the semi-infinite photonic crystal these oscillations form the band of the chiral Hall edge states (see Ref. 19). Likewise decreasing the cluster size reduces the number of the LDOS oscillations and broadens their width. The LDOS for the interface point of these two finite clusters can be four orders of magnitude greater than the free space value (see Fig. 4).

As reported in Ref. 19 the one-way Hall edge states exist for wavelengths in between these four bands [see Fig. 2(b)] of the corresponding infinite photonic crystals. These bands are represented as four peaks of the LDOS in Fig. 4 for a finite cluster. Therefore the scattering matrix **S** (15) must have poles for wavelengths in between these four peaks. We have searched for the poles of the scattering matrix for the cluster with $N_c = 770$ cylinders [see Fig. 1(a)] and have found a number of poles in this region. In particular there is a pole at the wavelength $\lambda/d = 4.436 + i0.015$ for the cluster shown in Fig. 1(a).

In Fig. 5 we plot the spatial profile of the magnetic field intensity $|H_z|^2$ of this mode. The energy flow of this mode is clockwise and a substantial part of the energy is leaked from the right-hand side of the cluster as the mode propagates clockwise. The quality factor of this mode is $Q = 140$. The field intensity $|H_z|^2$ of this one-way mode is localized at the right edge of the cluster. In contrast, the one-way mode for the corresponding semi-infinite photonic crystals is localized at their interface, which for this finite cluster is at $y/d = 11.3$.

To reduce the energy loss of this mode at the right edge of the cluster we have placed an additional mirror (with a band gap at these wavelengths) consisting of five layers of a hexagonal photonic crystal at the right-hand side of the cluster. We have found a chiral Hall edge state for this enlarged cluster of $N_c = 810$ cylinders at $\lambda/d = 4.439 + i0.009$. We have observed that now the leakage of the one-way edge mode is taking place from the bottom edge of the cluster (the plot is not provided). The quality factor of this mode is $Q = 245$. These high losses of the one-way modes in Fig. 5 and for a cluster with an additional mirror at the right-hand side occur because these modes exist for a frequency above the light line and therefore they need the support of mirrors to confine their
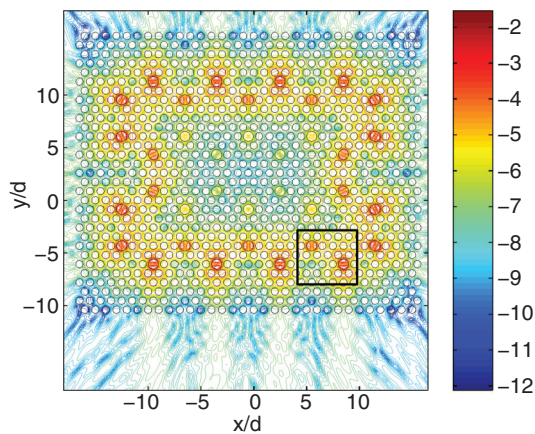
FIG. 6. (Color online) The intensity of the magnetic field distribution $|H_z|^2$ of the chiral Hall edge state for the gyroelectric cluster in the logarithmic scale at $\lambda/d = 4.435 + i4.617 \times 10^{-4}$. The quality factor of this mode is $Q = 48\,022$.

energy. This support occurs for semi-infinite photonic crystals where the one-way mode is localized at their interface.[19]

In Fig. 6 we plot $|H_z|^2$ as a function of position for a gyroelectric cluster surrounded by mirrors at all four edges. There are $N_c = 1007$ cylinders in this cluster. The one-way edge mode is confined at the interface of the gyroelectric cluster and mirrors (see Fig. 6), and the quality factor is substantially higher for this mode $Q = 48\,022$. The blue curve in Fig. 4 is the LDOS for this cluster and for the top black source point in Fig. 1(a). The LDOS is highly oscillatory in this case and each resonance corresponds to a one-way edge mode. To show the one-way nature of this mode in Fig. 7 we plot the distribution of the Poynting vector at the bottom right corner of the cluster. This plot shows the clockwise nature of the field propagation. Interestingly the energy flow inside the cylinders is anticlockwise. Such behavior might be determined by the geometry of the cluster but more calculations are needed before a general conclusion can be made. The field is concentrated
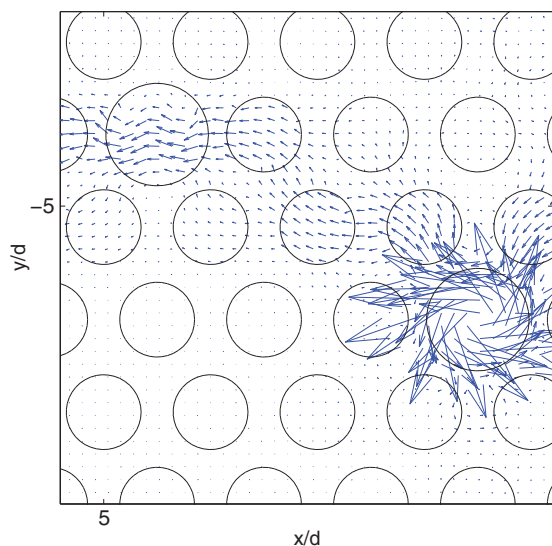

FIG. 7. (Color online) The map of the Poynting vector of the chiral Hall edge state of the outlined rectangular region in Fig. 6.
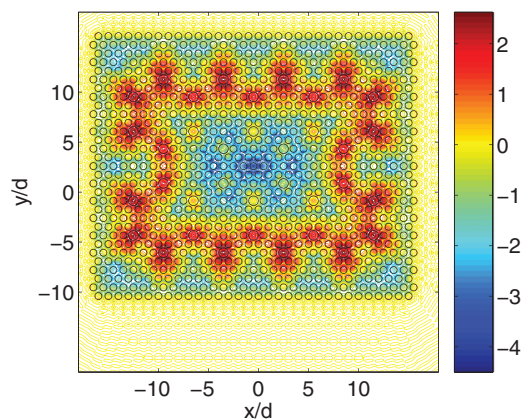

FIG. 8. (Color online) The LDOS ρ in the logarithmic scale versus position for one-way Hall state wavelength $\lambda = 4.435$.

more inside the gyroelectric cylinders. To excite this one-way mode, it is sufficient to place a radiating source close to the interface between these two clusters. We have calculated the field distribution for a source located at (0.5,11.65). The field distribution is very similar to the modal distribution (see Fig. 6) and we do not provide them here. Interestingly the field values inside of the gyroelectric cylinders and for a source oriented along the x axis are two orders of magnitude greater than for a y source orientation. This behavior can be explained by the fact that the x-oriented source matches the edge state field value and excites the edge state more easily than the y-oriented source at this source position.

In Fig. 8 we plot the spatial distribution of the LDOS for the chiral edge mode wavelength $\lambda = 4.435$ and for a cluster with $N_c = 1007$ cylinders. The LDOS is more than two orders of magnitude greater at the interfaces of the gyroelectric cluster and mirrors. The value of the LDOS is similar along the cluster's zigzag edges and armchair edges. Inside the cluster ρ diminishes and for this cluster it is four orders of magnitude smaller than the free space value.

The results shown demonstrate that the maximum value of the field intensity of chiral modes for finite clusters is not necessarily localized at the interface of photonic clusters (see Fig. 5). This information is important for the utilization of chiral edge modes in waveguiding, switching, and other applications. Surrounding a gyroelectric cluster with mirrors can create suitable conditions for photon storage and manipulation, which can be achieved by changing the strength of an external magnetic field.

B. LDOS and chiral Hall edge modes in ferrites clusters

In this section we study the properties of the LDOS and the chiral Hall edge modes in ferrite clusters. Here we use the parameters and geometry reported in Ref. 12 where it was shown that the one-way Hall states exist at the edge of the semi-infinite honeycomb ferrite photonic crystal and free space.

The honeycomb ribbon cluster [see Fig. 9(a)] is composed of a honeycomb lattice of yttrium-iron-garnet cylinders located in free space with radii $a = 0.2d$, where $d = 10$ mm is the lattice constant. The magnetic permeability tensor has the
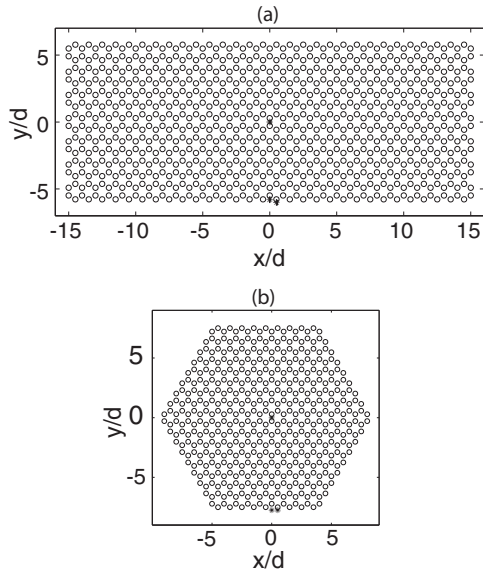
FIG. 9. The geometry of the ferrite clusters; (a) honeycomb ribbon, (b) honeycomb hexagonal flake.

form[27] with

$$\mu_\perp = 1 + \frac{\omega_0\omega_m}{\omega_0^2 - \omega^2}, \quad \mu_{xy} = \frac{\omega\omega_m}{\omega_0^2 - \omega^2}, \quad (16)$$

where $\omega_m = 4\pi\gamma M_s$ and $\omega_0 = \gamma H_0$. Here H_0 is the applied static magnetic field, $4\pi M_s$ is the saturation magnetization, and γ is the gyromagnetic ratio. Following Ref. 12 we have used the following values for these parameters: $4\pi M_s = 1750$ G, $H_0 = 500$ Oe with dielectric permittivity $\varepsilon = 15$. These are typical parameters for yttrium-iron-garnet ferrites (see Ref. 27). It is shown that the one-way Hall edge state can be excited at the wavelength $\lambda/d = 3.937$. This mode lies below the light line and is confined to the edge of the semi-infinite photonic crystal. Without magnetization ($\mu_\perp = 1$, and $\mu_{xy} = 0$) this infinite crystal has a degenerate Dirac point at the K point of the Brillouin zone. After magnetization the degeneracy at the K point is lifted and a band gap is opened. So the mechanism of the creation of the chiral Hall edge states is similar here to that for the gyroelectric example.

In Fig. 10(a) we plot the LDOS ρ as a function of wavelength for three different points located in free space, for a honeycomb ribbon with $N_c = 854$ cylinders plotted in Fig. 9(a). The bottom red solid curve is for a point at the center of the cluster [see the top black dot in Fig. 9(a)]. The LDOS ρ is three orders of magnitude lower than the free space value for this point. These low values for the LDOS are in accord with the existence of the band gap for a corresponding infinite photonic crystal. The middle blue dashed curve in Fig. 10 is the LDOS for the bottom left point in Fig. 9(a) and the green dotted top curve is for the bottom right point in Fig. 9(a). Although these points are located close to each other the difference between the LDOS values can be as high as two orders of magnitude. This implies that the LDOS is a sensitive function of position. The LDOS value for the point located at the zigzag edge inside the cylinder (not plotted here) is very similar to the LDOS value of the green dotted curve, except that it is
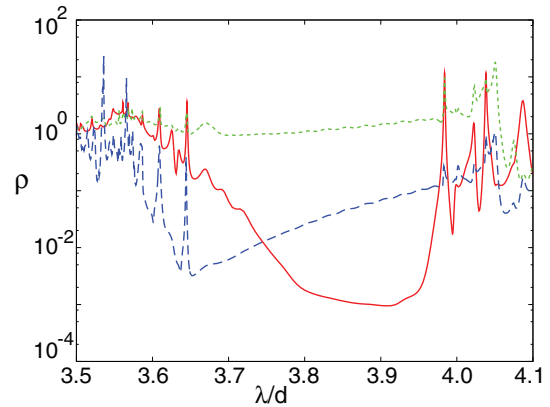

FIG. 10. (Color online) The LDOS ρ on a logarithmic scale vs wavelength λ/d for an observation point at the center of the cluster $(0,0)$ (red solid curve), for the zigzag edge points at $(0,-5.8)$ (blue dashed curve) and for the point $(0.5,-6.0)$ (green dotted curve). All points are located in free space.

an order of magnitude higher due to the higher value of the refractive index of the cylinders.

We have also calculated the LDOS for a honeycomb ribbon as in Fig. 9(a) but with twice the width. The qualitative behavior of the LDOS is very similar to Fig. 10 except for the point at the center where the LDOS is two orders of magnitude lower than in Fig. 10.

The LDOS values for the top green curve in Fig. 10 are nearly flat for the band-gap wavelengths $3.65 < \lambda/d < 3.95$, while the LDOS gradually increases for the middle blue curve. The chiral Hall edge states should exist within the band gap where we observe only very minute oscillations of the LDOS. We have searched for the poles in the complex plane for band-gap wavelengths and located one at $\lambda/d = 3.928 + i0.0177$. The real part of this pole is close to the edge state wavelength $\lambda/d = 3.937$ of a semi-infinite photonic crystal.[12] The Q factor of this chiral Hall edge state is $Q = 110$.

In Fig. 11 we plot the logarithm of the electric-field intensity $|E_z|^2$ distribution of this chiral Hall edge mode. The electric field of this mode is concentrated at the edges of the cluster and is maximal at the lower right corner and the upper left
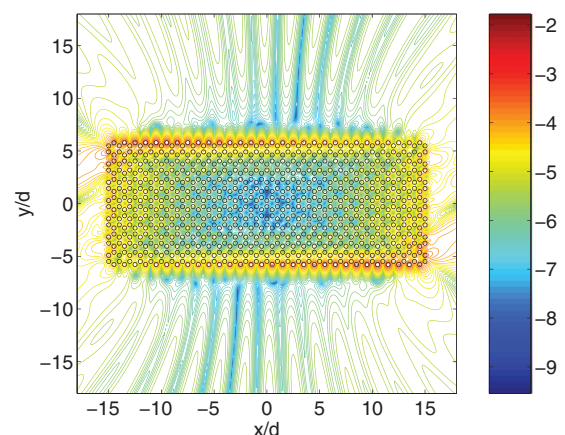

FIG. 11. (Color online) The intensity of the electric-field distribution $|E_z|^2$ in the logarithmic scale of the chiral Hall edge state for the honeycomb ribbon plotted in Fig. 9(a).
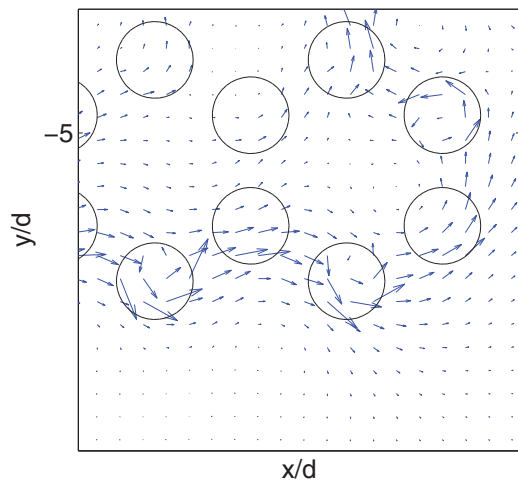
FIG. 12. (Color online) The fragment of the Poynting vector plot of the chiral edge mode plotted in Fig. 11 showing the unidirectional counterclockwise flow of energy at the bottom right edge of the ribbon.

FIG. 14. (Color online) The LDOS map in the logarithmic scale versus position for the chiral Hall edge state wavelength $\lambda'/d = 3.928$.

corner. The main "leakage" of the energy of this mode appears to be taking place at these corners. The values of $|E_z|^2$ diminish toward the center of the cluster and they are six orders of magnitude lower than at the edges of the cluster. The modal intensity is slightly stronger at the zigzag edges of the honeycomb ribbon than at the armchair edges for this configuration.

To show the unidirectional flow of energy in Fig. 12 we plot a fragment of the Poynting vector distribution for the bottom right corner of the ribbon which shows the way the chiral edge Hall mode propagates at the corner. When we swap the external magnetization to the opposite direction we find the pole at the same location as it should be but now the energy propagates in the clockwise direction and the maximum values of the electric-field intensity are reached at the top right and the bottom left corners of the ribbon.

To excite this one-way Hall edge state we used a point source located close to the zigzag edge of the cluster. In Fig. 13
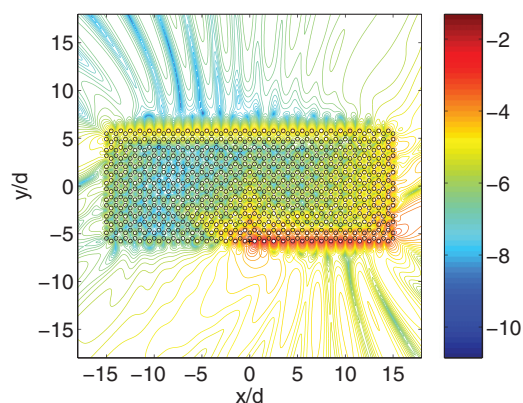

FIG. 13. (Color online) The spatial dependence of the Green's function, $|G|^2 = |E_z|^2$ in a logarithmic scale for a chiral edge state wavelength $\lambda/d = 3.928$ and for a source located at $(0.0, -5.8)$ (black dot in the plot) showing the excitation of the one-way Hall edge mode.
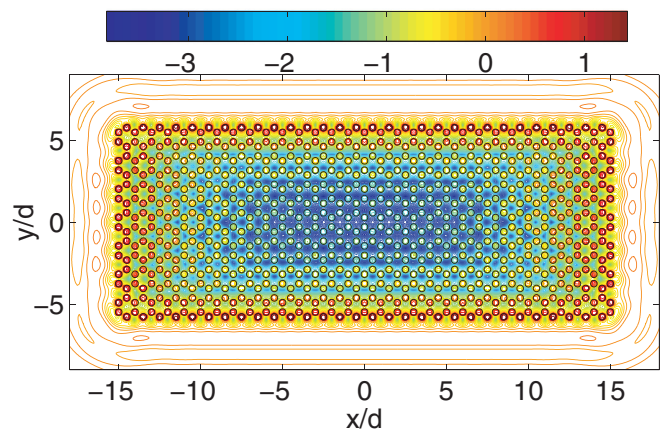
we present the electric-field intensity distribution showing the anticlockwise flow of energy. The wavelength of the radiation is equal to the real part of the corresponding pole wavelength value $\lambda'/d = 3.928$. The quality factor of this mode is not high and nearly all energy leaks out after one loop around the edge of the ribbon. If we change the direction of the magnetization then the energy flow will reverse, giving a convenient handle with which to control the direction of the propagation.

In Fig. 14, we plot the distribution of the LDOS for the chiral edge mode wavelength $\lambda'/d = 3.928$ as a function of position. The density of states more than an order of magnitude greater closer to the edges of the ribbon and diminishes toward the center of the ribbon. The values of the LDOS along the zigzag edges, and along the armchair edges, of the ribbon are comparable.

Now we consider the honeycomb hexagonal flake geometry [see Fig. 9(b)]. This cluster is composed of $N_c = 486$ cylinders and the cylinders are located at the honeycomb lattice points; the edges of the cluster itself have a hexagonal symmetry. The rest of the parameters are the same as in the previous example of the honeycomb ribbon. It is reported in Ref. 12 that such a cluster has a one-way edge state at $\lambda/d = 3.926$.

First in Fig. 15 we plot the LDOS as a function of wavelength. The red solid curve is for a point at the center of the flake at $(0.0, 0.0)$ while the green dotted curve and the blue dashed curve are for points at the bottom zigzag edge of the flake located at $(0.0, -7.75)$ and $(0.5, -7.75)$, respectively. In this case there are some resonances of the LDOS for gap wavelengths $3.65 < \lambda/d < 3.95$, even for an observation point near the center of the cluster. The oscillations are more pronounced for the point $(0.0, -7.75)$ which is located between the cylinders at the bottom zigzag edge and the resonances are very well developed for the point at $(0.5, -7.75)$. The number of resonances are the same for the top two curves. This is in strong contrast to the honeycomb ribbon case where the LDOS resonances inside the band gap are very weak (see Fig. 10). Such strong dependence of the LDOS on the shape of the cluster has been reported also for conventional clusters,[28] where the effects of the shape of the cluster on the Lamb shift and LDOS have been considered.
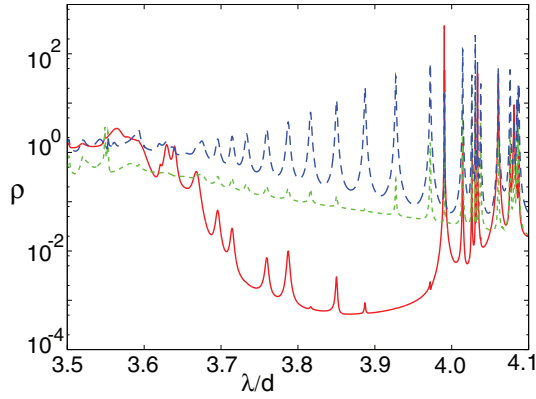
FIG. 15. (Color online) The LDOS ρ in the logarithmic scale vs wavelength λ/d for an observation point at the center of the cluster $(0,0)$ [top black dot in Fig. 9(b)] (red solid curve), for the zigzag edge points at $(0,-7.75)$ bottom left black dot in Fig. 9(b) (green dotted curve), and for the point $(0.5,-7.75)$ bottom right black dot in Fig. 9(b) (blue dashed curve). All points are in free space.

We searched for poles and as expected we found poles close to these LDOS resonance wavelengths. In Fig. 16 we plot the one-way Hall edge mode for the pole value $\lambda/d = 3.927 + i6.875 \times 10^{-4}$. The quality factor of this mode is $Q = 2856$ which is much higher than the mode for the honeycomb ribbon. Overall the spatial behavior of this mode is very similar to the mode of the honeycomb ribbon. The field mainly concentrates at the edges of the cluster and its value diminishes toward the center of the flake. The energy flow for this mode is anticlockwise. To excite this mode it is sufficient to place a point source with a radiation wavelength equal to the real part of the corresponding pole wavelength near the flake edge.[12]

Finally in Fig. 17 we plot the LDOS map as a function of position in the logarithmic scale for chiral edge wavelength $\lambda/d = 3.927$. The LDOS is two orders of magnitude greater at the edges of the flake and it diminishes toward the center of the flake. This behavior of the LDOS is similar to the honeycomb ribbon case. Such a spatial distribution of ρ is reminiscent of topological insulators which have metallic surfaces (high

FIG. 17. (Color online) The LDOS map in the logarithmic scale versus position for chiral Hall edge state wavelength $\lambda/d = 3.927$.

density of states) and insulating bulk (low density of states) although they have different topological invariants.[29]

One of the intrinsic properties of the chiral Hall edge states is their immunity to disorder. We have introduced radial disorder in which the radii of all honeycomb flake cluster cylinders are disordered [Fig. 9(b)]. In our calculation the radii of cylinders have been uniformly distributed in the range $[0.13d, 0.2d]$ which corresponds to a 35% degree of disorder from the initial value $a = 0.2d$. In such strong radial disorder guiding is no longer taking place in conventional photonic crystal waveguides.[30] Here however the resonances of the LDOS representing chiral Hall edge states largely withstand such strong disorder (see green dotted line in Fig. 18). The resonances are broadened and their maximum values are reduced and shifted toward shorter wavelengths while the number of peaks are essentially preserved. We have also considered radial disorder in which only the radii of the bottom row of the honeycomb flake cluster cylinders are disordered [Fig. 9(b)]. In this calculation the radii of the cylinders have been uniformly distributed in the range $[0.05d, 0.2d]$ which corresponds to a 75% (one-sided) degree of disorder. The
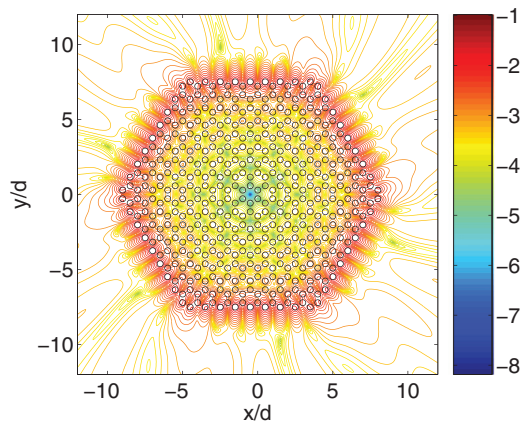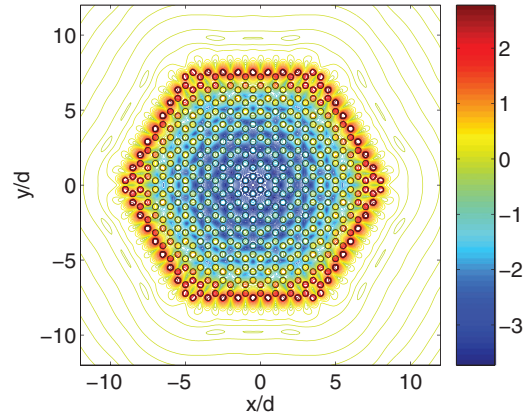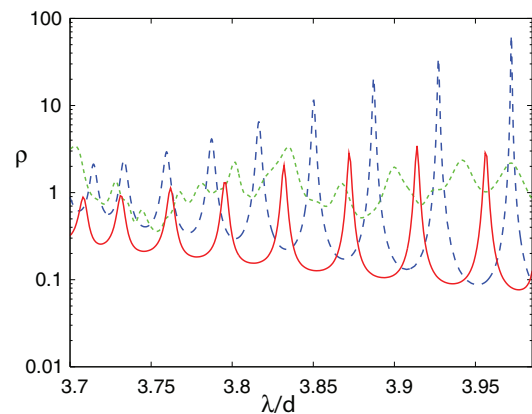

FIG. 16. (Color online) The intensity of the electric-field distribution $|E_z|^2$ in the logarithmic scale of the chiral Hall edge state for the honeycomb flake with $\lambda/d = 3.927 + i6.875 \times 10^{-4}$.

FIG. 18. (Color online) The LDOS ρ on the logarithmic scale as a function of wavelength λ/d for the bottom right point on Fig. 9(b); the blue dashed curve is the same blue dashed curve as in Fig. 15, the green dotted line is for 35% degree of radial disorder for all cluster cylinders, while the red solid line is for a cluster with the 75% degree of radial disorder of the bottom row of cylinders only in Fig. 9(b).

resonances of the LDOS withstand such strong disorder also (see the red solid line in Fig. 18). The resonances are simply shifted toward short wavelengths but their number is preserved and their quality factors do not change substantially.

IV. CONCLUSIONS

We have constructed the Green's tensor using a multipole approach and have calculated the LDOS of chiral Hall edge states for finite photonic gyrotropic clusters. The multipole method has proven to be very accurate and effective. Both ferrites and gyroelectric photonic clusters have been treated.

For a honeycomb ribbon, honeycomb hexagonal flake, and square photonic clusters with embedded honeycomb gyroelectric resonators, we have calculated the LDOS as a function of wavelength, position, shape, and the size of the cluster. It is shown that the LDOS is a sensitive function of the position and the shape of the cluster. The LDOS at the edges of the ferrite clusters can have low values even at the chiral edge state wavelengths. For the ferrite honeycomb ribbon these low values of the LDOS are located between the cylinders at either the armchair edges or at the zigzag edges of the ribbon or at the zigzag edges of the honeycomb flake (see Figs. 14 and 17). The LDOS along the zigzag edges and armchair edges of both gyroelectric and ferrite clusters are similar at one-way edge wavelengths.

The LDOS value at the one-way edge state wavelengths can be orders of magnitude higher at the edges of the cluster compared with its free space value, while its value diminishes toward the center of the cluster. This property of the LDOS at one-way edge state wavelengths ensures high edge transmission (conductance) and insulating bulk in such clusters. Therefore the conductance properties of such clusters have some resemblance to those of topological insulators.[29]

The spatial distribution of chiral Hall modes and their quality factors have been calculated for both gyroelectric and ferrites clusters. The spatial distribution of these modes is not necessarily localized at the edges of the cluster. The modal field can be localized at the "leaking edges" of the cluster rather than at the interface of two clusters as in the semi-infinite photonic crystals case. We have observed such behavior for gyroelectric clusters.

For ferrites clusters the chiral modes are localized uniformly at the edges of the honeycomb hexagonal flake while for the honeycomb ribbon the modes are localized more at two diagonally opposite corners and their modal intensity distribution depends on the direction of the external magnetic field. We have also observed strong immunity of the LDOS to disorder. Strong radial disorder blueshifts the LDOS resonances but does not change their number and their quality factors substantially.

The results presented here are important for designing chiral edge state based waveguide interconnects, delay waveguides, as well as in photon storage and manipulation applications. These findings can also be used for understanding chiral mode excitations and the characterization of radiation dynamics of sources embedded in such clusters. The results for the spatial distribution of chiral Hall edge modes may also be useful in electronic systems given that the photonic chiral modes are the direct analog of the electronic Hall edge states.

*Corresponding author: ara.asatrian@uts.edu.au

[1] J. D. Joannopoulos, S. G. Johnson, J. N. Winn, and R. D. Meade, *Photonic crystals: Molding the Flow of Light* (Princeton University Press, Princeton, NJ, 2008).

[2] K. von Klitzing, G. Dorda, and M. Pepper, Phys. Rev. Lett. **45**, 494 (1980).

[3] R. B. Laughlin, Phys. Rev. B **23**, 5632 (1981).

[4] D. J. Thouless, M. Kohmoto, M. P. Nightingale, and M. den Nijs, Phys. Rev. Lett. **49**, 405 (1982).

[5] B. I. Halperin, Phys. Rev. B **25**, 2185 (1982).

[6] F. D. M. Haldane, Phys. Rev. Lett. **61**, 2015 (1988).

[7] F. D. M. Haldane and S. Raghu, Phys. Rev. Lett. **100**, 013904 (2008).

[8] S. Raghu and F. D. M. Haldane, Phys. Rev. A **78**, 033834 (2008).

[9] Z. Wang, Y. D. Chong, J. D. Joannopoulos, and M. Soljacic, Phys. Rev. Lett. **100**, 013905 (2008).

[10] Z. Wang, Y. D. Chong, J. D. Joannopoulos, and M. Soljacic, Nature (London) **461**, 772 (2009).

[11] B. Simon, Phys. Rev. Lett. **51**, 2167 (1983).

[12] X. Ao, Z. Lin, and C. T. Chan, Phys. Rev. B **80**, 033105 (2009).

[13] Z. Yu, G. Veronis, Z. Wang, and S. Fan, Phys. Rev. Lett. **100**, 023902 (2008).

[14] T. Ochiai and M. Onoda, Phys. Rev. B **80**, 155103 (2009).

[15] Y. Mazor and B. Z. Steinberg, Phys. Rev. B **86**, 045120 (2012).

[16] Y. Hadad and B. Z. Steinberg, Phys. Rev. Lett. **105**, 233904 (2010).

[17] Y. Hadad, Y. Mazor, and B. Z. Steinberg, Phys. Rev. B **87**, 035130 (2013).

[18] H. Zhu and C. Jiang, Opt. Express **18**, 6914 (2010).

[19] K. Fang, Z. Yu, and S. Fan, Phys. Rev. B **84**, 075477 (2011).

[20] R. Balian and C. Bloch, Ann. Phys. **64**, 271 (1971).

[21] E. N. Economou, *Green's Functions in Quantum Physics* (Springer-Verlag, Berlin, 2006).

[22] A. A. Asatryan, K. Busch, R. C. McPhedran, L. C. Botten, C. M. de Sterke, and N. A. Nicorovici, Waves Random Media **13**, 9 (2003).

[23] A. A. Asatryan, K. Busch, R. C. McPhedran, L. C. Botten, C. M. de Sterke, and N. A. Nicorovici, Phys. Rev. E **63**, 046612 (2001).

[24] A. A. Asatryan, S. Fabre, K. Busch, R. C. McPhedran, L. C. Botten, C. M. de Sterke, and N. A. Nicorovici, Opt. Express 8, 191 (2001).

[25] J. A. Kong, *Electromagnetic Wave Theory* (EMW, Cambridge, MA, 2005).

[26] Y. Hatsugai, Phys. Rev. Lett. 71, 3697 (1993).

[27] D. M. Pozar, *Microwave Engineering* (Wiley, New York, 1988).

[28] A. A. Asatryan, L. C. Botten, N. A. Nicorovici, R. C. McPhedran, and C. M. de Sterke, Waves Random Complex Media 16, 151 (2006).

[29] X.-L. Qi and S.-C. Zhang, Rev. Mod. Phys. 83, 1057 (2011).

[30] T. N. Langtry, A. A. Asatryan, L. C. Botten, C. M. de Sterke, R. C. McPhedran, and P. A. Robinson, Phys. Rev. E 68, 026611 (2003).